Chinese Chemical Letters 36 (2025) 109860

Contents lists available at ScienceDirect

Chinese Chemical Letters

journal homepage: www.elsevier.com/locate/cclet

A novel and visible ratiometric fluorescence determination of carbaryl based on red emissive carbon dots by a solvent-free method

Meiling Xu[a], Xinyang Li[a], Pengyuan Liu[b], Junjun Liu[b], Xiao Han[b], Guodong Chai[a], Shuangling Zhong[a,c], Bai Yang[b,*], Liying Cui[a,c,*]

[a] College of Resources and Environment, Jilin Agricultural University, Changchun 130118, China
[b] State Key Laboratory of Supramolecular Structure and Materials, College of Chemistry, Jilin University, Changchun 130012, China
[c] Key Laboratory of Straw Biology and Utilization, The Ministry of Education, Jilin Agricultural University, Changchun 130118, China

ARTICLE INFO

Article history:
Received 25 January 2024
Revised 29 March 2024
Accepted 3 April 2024
Available online 4 April 2024

Keywords:
Carbon dots
Visual detection
Fluorescence sensor
Quantum yield
Carbaryl detection

ABSTRACT

In this study, a simple and effective ratiometric fluorescence method has been developed for carbaryl detection, utilizing red emissive carbon dots (R-CDs). The underlying principle of this proposed strategy relies on the rapid hydrolysis of carbaryl under an alkaline condition and production of 1-naphthol with blue-emission at 462 nm. Furthermore, the as-synthesized R-CDs (Em. 677 nm), serve as a reference, enhancing the visual tracking of carbaryl through the transformation of fluorescent color from red to blue. The concentration of carbaryl exhibits a commendable linear correlation with the ratio of fluorescence intensity, ranging from 0 to 20 μg/mL ($R^2 = 0.9989$) with a low detection limit of 0.52 ng/mL. Additionally, the described methodology can be used for the enzyme-free visual assay of carbaryl, even in the presence of other carbamate pesticides and metal ions, in tap water and lake water samples with excellent accuracy (spiked recoveries, 94%–106.1%), high precision (relative standard deviation (RSD) $\leq$ 2.42), and remarkable selectivity. This fast and highly sensitive naked-eye ratiometric sensor holds immense promise for carbaryl detection in intricate environments and food safety fields.

Carbaryl, a typical carbamate introduced in the late 1950s, is extensively applied in agriculture because of its capability in combating a wide spectrum of pernicious insect species [1,2]. However, due to the excessive and escalated employment over the past decades, carbaryl residue implies a serious threat to environment and human health *via* contamination of ground and surface water. In order to mitigate these potential risks, it is very necessary to monitor carbaryl residue. So far, a wide variety of analytical techniques have been explored to discriminate and quantify the presence of carbaryl in food and water, such as liquid chromatography-mass spectrometry [3,4], gas chromatography-mass spectrometry [5], electrochemical analysis [6,7], and surface-enhanced Raman spectroscopy [8,9]. Although these methods have excellent selectivity and sensitivity, most of these techniques suffer from the shortcomings of expensive instruments, time-consuming sample pretreatment, skilled operators, and cumbersome experimental operations [10,11]. Therefore, the wide-scale implementation of these traditional techniques is severely limited. Alternatively, sensor-based fluorescent nanomaterials have emerged as a promising approach to surmount the aforementioned obstacles, thereby promising breakthrough in this field.

Recently, fluorescent nanomaterials have attracted great attention and have been the subject of extensive research in detecting carbaryl, because of their distinctive optical properties. Currently, involving fluorescent nanomaterials mainly encompasses quantum dots (QDs) [12–16], metal nanoclusters [17,18] and carbon dots (CDs) [19–23]. On the basis of QDs with good light stability, there are a few reports concerning the recognition of carbaryl based on QDs. For example, Zhang *et al*. pioneered the construction of fluorescence sensing materials based on CdSe/ZnS QDs and molecularly imprinted polymer (MIP) for identifying carbaryl in rice and Chinese cabbage [12]. The sensing mechanism relies on the selective recognition and binding of carbaryl with QDs@MIP, leading to fluorescence quenching. Chen *et al*. further promoted the development of QDs in this field by fabricating a visual sensor using CdTe QDs and nano porphyrins, adopting a "turn-off-on" mode to selectively determine carbaryl in different food matrices [13]. Moreover, Shahdost-fard *et al*. designed a ratiometric fluorescence strategy employing CdTe QDs for the naked-eye detection of carbaryl in apple [14]. However, QDs containing heavy metal ions inher-

* Corresponding authors.
E-mail addresses: byangchem@jlu.edu.cn (B. Yang), cuily@iccas.ac.cn (L. Cui).

https://doi.org/10.1016/j.cclet.2024.109860
1001-8417/

ently impose certain limitations, such as toxicity and chemical instability, thereby impeding their further application [16]. As members of metal nanomaterials, gold nanoparticle-based colorimetric assays have been proposed as an alternative for monitoring the level of carbaryl with dual readouts (colorimetric and fluorometric) in complex solutions. Nonetheless, this sensor strategy is conspicuously cost-intensive [17]. Hence, it is crucial to explore cost-effective and eco-friendly nanomaterials for fabricating highly sensitive and selective fluorescent sensors.

CDs, one of the particularly popular representatives of fluorescent nanomaterials, can be easily obtained through various synthesis methods and numerous precursors [24–26]. CDs have been widely applied in fluorescent analysis [27], optoelectronic devices [28–30] and biomedical imaging [31], due to their outstanding photostability, excellent biocompatibility and strong fluorescence [32,33]. However, research on the fluorescence sensor of carbaryl based on CDs is limited. For instance, Li *et al.* demonstrated carbaryl detection by incorporating CDs into a complex two-enzyme coupled reaction system [19]. Subsequently, a dual-mode sensor with colorimetric and fluorometric readout for discriminating carbaryl was established through single-enzyme detection system [20,21]. The sensing mechanism focused on the non-fluorescence state of CDs resulting from the inner filter effect of silver or gold nanoparticles, and combining with the catalysis of acetylcholinesterase. This detection method exhibited high accuracy and reliability when applied to the determination of carbaryl in real samples. However, above analytical strategies heavily rely on enzyme inhibition and still face certain challenges. One is that enzymes are susceptible to inactivation, thereby affecting the sensitivity, accuracy, and practicability of fluorescent sensors [34]. Another is the difficulty in achieving precise quantitative readout due to the visual detection effect [35]. Therefore, developing CDs-based enzyme-free detection for carbaryl remains a formidable task.

In general, the traditional fluorescence-based method based on a single fluorescent signal is subject to interference from background absorption, light source fluctuations, fluorescent probes, and environmental conditions [36]. The ratiometric fluorescence sensor possesses the ability of self-calibration by measuring two fluorescence signals. It effectively enhances stability, accuracy, and sensitivity while providing a diverse range of colors for visible detection [37,38]. For example, Wang *et al.* constructed a ratiometric fluorescence sensor for detecting carbaryl by confining CDs in SiO_2 nanoparticles [22]. The CDs were synthesized by a simple hydrothermal method, emitting a blue fluorescence as reference signal readout in aqueous solution. This detection system also achieved simultaneous identification of carbaryl, thiram and chlorpyrifos through multi-channel analysis. Yang *et al.* achieved ratiometric fluorescent detection for carbaryl (50.00–1100.00 μmol/L) utilizing green-emission CDs [23]. Notably, a striking color variation from green to blue was observed, and the detection limit was determined to be 1.11 μmol/L. However, the optical application of CDs with blue or green light emission is severely hindered due to autofluorescence or background interference in complex matrices [39]. Therefore, achieving high-efficient red-emission CDs has become one of the challenging tasks in fluorescence recognition of carbaryl.

In this study, an enzyme-free ratiometric fluorescent platform has been developed using red-emission CDs (R-CDs) (Em. 677 nm) for carbaryl detection. R-CDs were synthesized through a facile, solvent-free carbonization method using taxus, a natural biomass, as carbon source. R-CDs exhibited an impressive quantum yield of 22.3%. Interestingly, under alkaline condition, methyl isocyanate group of carbaryl would be hydrolyzed by SN2 substitution reaction to produce blue-emission 1-naphthol (Em. 462 nm). It is known that distinguishing color variations with the naked eye at low concentrations is challenging. To circumvent this limitation, R-CDs were incorporated into a ratiometric fluorescence sensing system owning dual-emission peaks at 462 and 677 nm. Remarkably, with a single-wavelength excitation at 365 nm, the visual detection of carbaryl (transformation from red to blue) could be reliably achieved by the naked eye. This expeditious sensing strategy was successfully applied to determine carbaryl in both tap water and lake water, yielding results of high precision and accuracy.

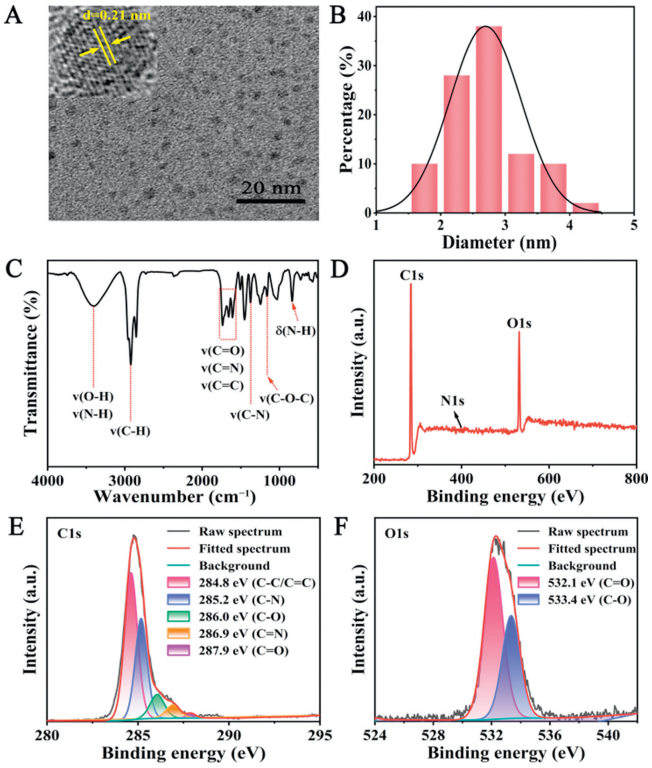

Fig. 1. (A) TEM and (inset) high-resolution TEM images of R-CDs. (B) Histogram of the size distribution of R-CDs. (C) FT-IR spectrum of R-CDs. (D) XPS survey spectrum of R-CDs. High-resolution XPS spectra of C 1s (E) and O 1s (F).

R-CDs derived from taxus leaves (Scheme S1 in Supporting information) were synthesized at 120 °C for 3 h by a one-step solvent-free carbonization method, resulting in a production yield of *ca.* 5%. The morphological characterization and size of as-synthesized R-CDs were examined using transmission electron microscopy (TEM) (Fig. 1A). R-CDs present a well-dispersed spherical shape with an average particle size of 2.7 ± 0.5 nm. The high-resolution TEM image reveals a distinct lattice spacing value of 0.21 nm, which is consistent with the (100) graphite plane [40]. The size distribution of R-CDs ranges from 1.7 nm to 4.1 nm (Fig. 1B). The X-ray diffraction (XRD) pattern of R-CDs exhibits a characteristic peak at around 19.5° and can be ascribed to the (002) planes of graphitized carbon, which is in accord with the HRTEM results (Fig. S1 in Supporting information) [41]. Fourier transform infrared (FT-IR) spectrum (Fig. 1C) was conducted to identify the surface functional groups of R-CDs. The peak at 3415 cm^{-1} signifies the characteristic absorption of O–H/N–H stretching vibration, indicating the presence of hydroxyl and amino groups on the surface of R-CDs, respectively [42]. The peak at 2924 cm^{-1} is assigned to the stretching vibration of C–H. The absorption bands of C=O and C=N vibration can be observed at 1735 and 1656 cm^{-1}, respectively [43]. The absorption peak at 1607 cm^{-1} is attributed to the stretching vibration of C=C bonds in benzene rings [44]. Two distinct peaks at 1374 and 1160 cm^{-1} can be ascribed to the stretching vibrations of C-N and C-O-C, respectively. Furthermore,

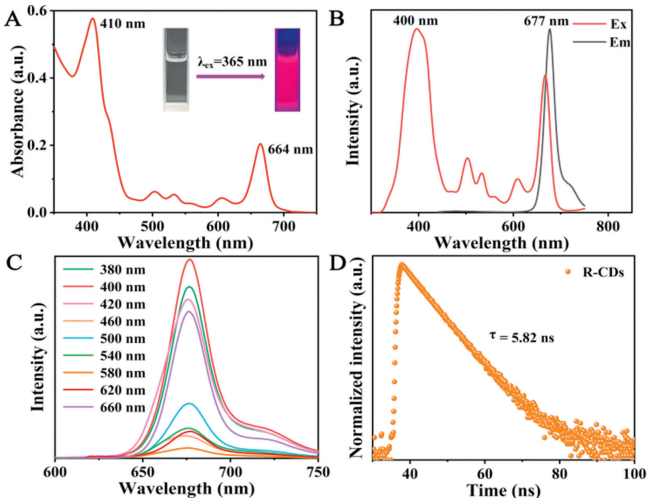

Fig. 2. (A) UV–vis absorption spectrum, inset: the photograph of R-CDs in acetone solution (0.1 mg/mL) under daylight (left) and UV light (right). (B) Excitation and emission spectra of R-CDs. (C) Fluorescent spectra of R-CDs upon excitation at different wavelengths from 380 nm to 660 nm. (D) Fluorescence lifetime of R-CDs at 677 nm.

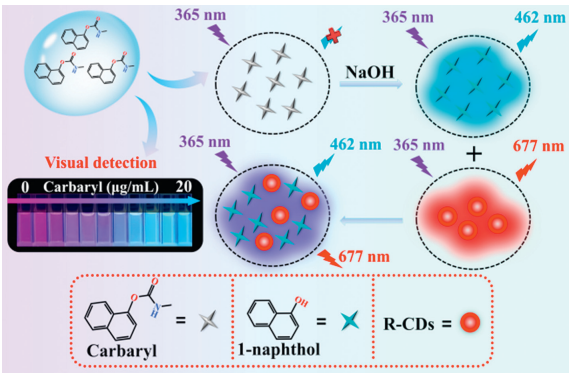

Scheme 1. Sensing strategy of the proposed ratiometric fluorescence sensor using R-CDs for carbaryl detection.

the peak around 837 cm^{-1} represents the bending vibrations of N–H bonds.

Surface analysis of R-CDs was performed using X-ray photoelectron spectroscopy (XPS) (Fig. 1D). The C 1s, N 1s and O 1s peaks are observed at 284.8, 402.8 and 531.8 eV, respectively. The high-resolution C 1s spectrum (Fig. 1E) reveals five distinct forms of carbon: C-C/C=C (284.8 eV), C-N (285.2 eV), C-O (286.0 eV), C=N (286.9 eV), and C=O (287.9 eV) [45,46]. The O 1s spectrum (Fig. 1F) exhibits two peaks at 532.1 and 533.4, corresponding to the contribution of C=O and C-O [47]. The XPS results are in consistence with those obtained from FT-IR, both demonstrating the presence of carboxyl, hydroxyl, and amino groups on the surface of R-CDs [48]. In addition, according to the full XPS spectrum (Fig. 1D), it can be concluded that R-CDs primarily comprise C (67.57%, atomic percentage), N (1.20%, atomic percentage), and O (31.23%, atomic percentage), which aligns with the elemental analysis data (Table S1 in Supporting information).

The optical performance of as-synthesized R-CDs was evaluated by ultraviolet–visible (UV–vis) absorption and photoluminescence measurements. The UV–vis spectrum (Fig. 2A) of R-CDs solution exhibits a remarkably broad absorption range, spanning from UV to deep red light regions, with two characteristic peaks at 410 and 664 nm. These peaks can be ascribed to the n-π^* transition of C=N/C=O bonds from porphin structure [49]. When exposed to UV irradiation (365 nm), the prepared R-CDs emit a striking deep red fluorescence, while appearing almost colorless under visible light condition (inset of Fig. 2A). The corresponding excitation and emission spectra of R-CDs display well-defined peaks at 400 nm and 677 nm, respectively (Fig. 2B). Fig. 2C displays the emission spectra associated with various excited illumination. It is observed that the emission peak position remains basically in the same position under different excitation wavelengths. Additionally, the fluorescence lifetime is approximately 5.82 ns (Fig. 2D). The optical properties and fluorescence lifetime of R-CDs are similar to those of chlorophyll a (Fig. S2 in Supporting information). This indicates the luminous centers of R-CDs are derived from chlorophyll, which is consistent with recent report [50]. The absolute quantum yield of deep red emissive R-CDs in acetone reaches an impressive value of 22.3% under the optimal excitation wavelength of 410 nm. However, that of the chlorophyll a solution is only 4.2%. Due to optical stability remarkably related to the precision and repeatability, the performances of R-CDs were assessed at different pH and ionic strength (Fig. S3 in Supporting information). Notably, R-CDs exhibit outstanding photostability within a pH range of 8.0–10.0 and a NaCl concentration range of 0.1–1.0 mol/L, indicating their excellent durability even in high ionic strength environment. However, it is observed that the fluorescence intensities of R-CDs decrease under strong acidic or alkaline conditions, likely due to the dissociation or protonation of the surface functional groups [51]. Therefore, the prominent optical performance of R-CDs ensures the accurate and reliable sensing in various practical applications.

The principle of the proposed strategy relies on the rapid hydrolysis of carbaryl in an alkaline environment and the subsequent production of 1-naphthol with blue emission at 462 nm. Besides, using R-CDs with red emission at 677 nm, as a reference, improves the sensitivity and visual tracking of carbaryl by transitioning emission color tonality from red to blue (Scheme 1). In order to gain further insights into the underlying mechanism of this strategy, the fluorescence spectra, UV–vis absorbance spectra and fluorescence lifetime decay spectra of various solutions were investigated (Figs. S4–S7 in Supporting information). Under 365 nm excitation, R-CDs exhibit a distinct emission peak at 677 nm. The fluorescence intensity at 677 nm shows a slight decrease upon the addition of NaOH (0.01 mol/L) to R-CDs (Fig. S4). Carbaryl (9 μg/mL) alone does not exhibit any fluorescence signal. However, in an alkaline condition, the hydrolysis product of carbaryl displays a sharp emission signal at 462 nm with remarkable blue emission. As the carbaryl concentrations increase with the presence of R-CDs, the emission peaks at 677 nm remain relatively constant (Fig. S5), while the fluorescent intensities at 462 nm regularly increase. Based on these observations, we consider that ratiometric detection of carbaryl could be achieved by the introduction of R-CDs. In additon, the UV–vis absorbance of R-CDs shows a small overlapping with the emission spectra of 1-naphthol (Fig. S4), which means that fluorescence resonance energy transfer (FRET) between 1-naphthol and R-CDs exists. Fluorescence lifetime of 1-naphthol changes from 8.43 ns to 6.54 ns after adding R-CDs, which further confirms the existence of FRET (Fig. S6).

A series of experimental conditions including R-CDs volume, NaOH concentration and incubation time, were optimized to achieve the optimal sensing performance of ratiometric detection of carbaryl. The appropriate ratio of two fluorophores plays a crucial role in generating a wide range of color change, hence the initial focus is on optimizing the volume of R-CDs. As shown in Fig. S8A (Supporting information), a negative correlation is observed between the ratiometric signal of I_{462}/I_{677} and R-CDs volume in the range of 30–190 μL at varying carbaryl concentrations. The signal approaches a constant value after the addition of 100 μL R-CDs. For the purpose of achieving the best visual effect, a R-CDs volume of

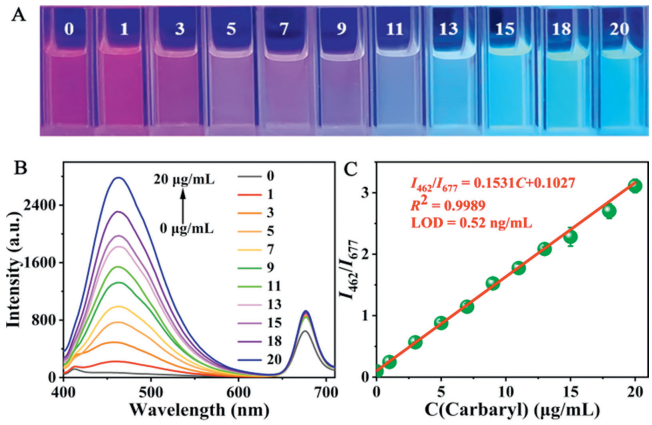

Fig. 3. (A) The fluorescence images of the ratiometric sensor (R-CDs and 1-naphthol) under UV lamp. (B) Ratiometric response (I_{462}/I_{677}) under optimum conditions, and (C) the linear relationship between the fluorescence intensity ratio (I_{462}/I_{677}) and different concentrations of carbaryl at a range of 0–20 μg/mL.

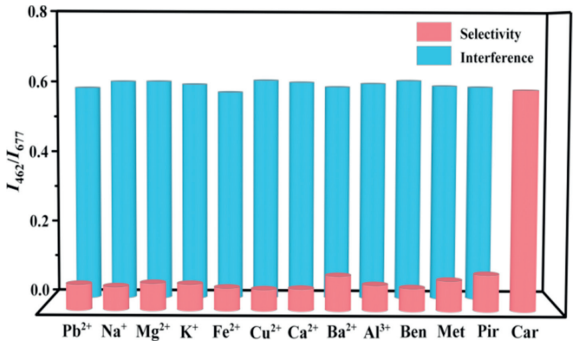

Fig. 4. Bar plots of fluorescence response of the carbaryl sensor in the presence of common interfering metal ions and pesticides.

Table 1
The determination of carbaryl in environmental water samples.

Sample	Spiked (μg/mL)	Found (μg/mL)	Recovery (n = 3,%)	RSD (n = 3,%)
Tap water	3	2.88	96.0	1.42
	9	9.55	106.1	0.48
	15	14.44	96.3	1.53
Lake water	3	2.82	94.0	2.42
	9	9.04	100.4	1.73
	15	14.36	95.7	0.92

100 μL is selected for further experiments. According to the literatures, it is known that the hydrolysis of carbaryl occurs rapidly in highly alkaline environment, which serves as the basis for our proposed detection strategy [52,53]. And the concentration of NaOH plays an important role in the color change and detection performance. The ratiometric response is measured in the presence of varying NaOH volume from 0 μL to 600 μL (Fig. S8B in Supporting information). The influence of the ratio of R-CDs to NaOH volume on visualization was also investigated (Fig. S9 in Supporting information). Considering comprehensively, the optimum NaOH volume of 500 μL was chosen. To evaluate the sensor response speed, the ratiometric signals were studied at various time intervals following the addition of carbaryl. Apparently, the ratiometric response is almost constant after 6 min (Fig. S10 in Supporting information). Therefore, the fluorescence spectra were measured after 6 min. The sensor exhibits a rapid response within the field of pesticide monitoring.

One of the prominent advantages of the proposed ratiometric approach in this study is the achievement of simple visual sensing of carbaryl based on a combination of the emission colors of 1-naphthol and R-CDs. Utilizing R-CDs in the presence of varying concentrations of 1-naphthol yields a wide spectrum of color variations ranging from red to purple and to blue under 365 nm UV light. Obvious color variations are observed for carbaryl detection from red to blue, which can be visualized by naked eye (Fig. 3A). To further enhance the precision and dependability, a ratiometric fluorescence sensor taking advantage of ratio of two fluorescence intensities at two different wavelengths was employed. As the concentration of carbaryl increases from 0 μg/mL to 20 μg/mL, the fluorescent signal emitted by 1-naphthol hydrolyzed from carbaryl at 462 nm displays a gradual augmentation, while the signal emitted by R-CDs at 677 nm remains relatively constant (Fig. 3B). The calculated I_{462}/I_{677} values exhibit a good linear relationship with the carbaryl concentrations, thereby attesting to the viability of employing the ratiometric approach for detecting carbaryl (Fig. 3C). Under a regression equation of $I_{462}/I_{677} = 0.1531C + 0.1027$ ($R^2 = 0.9989$), the LOD value is determined to be 0.52 ng/mL based on $3\sigma/K$, where σ is the standard deviation of six consecutive scans of the blank sample and K denotes the slope of the calibration curve of the ratiometric sensor [54]. It is noteworthy that the proposed method in this study exhibits excellent repeatability. The calculated LOD value is significantly lower than the maximum residue limit of carbaryl according to the Chinese drinking water quality standard (GB2763–2016) (0.05 mg/L), European Union (0.05 mg/L) and United States (0.02 mg/L) pesticides database [19], as well as numerous other established methods for carbaryl detection across a diversity of real samples. A comprehensive comparison of various methodologies implemented for the determination of carbaryl has already been presented in Table S2 (Supporting information). More importantly, this straightforward, expeditious, and enzyme-free methodology for visual detection of carbaryl represents an extraordinary breakthrough in the field of food industry and environmental pollution monitoring with far-reaching implication.

In order to evaluate the selectivity and anti-interference ability of the ratiometric fluorescent sensor designed for carbaryl detection, an investigation into the impacts of various common potentially interfering substances was conducted. It is well-known that different metal ions and other pesticides can exert significant influence on the detection performance. Therefore, the effects of representative metal ions, such as Pb^{2+}, Na^{+}, Mg^{2+}, K^{+}, Fe^{2+}, Cu^{2+}, Ca^{2+}, Ba^{2+}, Al^{3+}, as well as carbamate pesticides including benfuracarb (Ben), metolcarb (Met), primicarb (Pri) on the detection performance were examined. The results clearly demonstrate the exceptional selectivity of R-CDs-based sensor for carbaryl (Fig. 4). Furthermore, a mixture consisting of carbaryl and the aforementioned interfering substances individually into the R-CDs sensor system was investigated. Compared to carbaryl alone, the effects of these interfering substances on the recognition of carbaryl are found to be negligible. The outstanding selectivity and anti-interference imply promising potential for carbaryl detection in real samples.

To assess the effectiveness of the strategy in detecting real samples, carbaryl residues in tap water and lake water were analyzed utilizing the sensing platform. As shown in Table 1, no traces of carbaryl residues are detected in real samples. After spiked with different concentrations of carbaryl, satisfactory recoveries (96.0%–106.1% for tap water, 94.0%–100.4% for lake water) with relative standard deviation (RSD) values less than 2.42% are presented. The remarkable and excellent performance demonstrates that the ratiometric fluorescent sensing system is not only proficient but also practical for the visual detection of carbaryl in real samples.

A facile, enzyme-free, and cost-effective ratiometric fluorescent sensing system has been established for carbaryl detection with

high sensitivity and selectivity. This innovative approach builds on the understanding that the hydrolyzed derivative of carbaryl in alkaline conditions exhibits blue emission at 462 nm. Furthermore, R-CDs with red emission at 677 nm as an internal reference are used to construct a ratiometric fluorescent system and facilitate the visual sensing of carbaryl through obvious fluorescent color changes from red, purple to blue. Preliminary results imply broad linearity of the calibration curve for carbaryl detection with a low LOD and acceptable accuracy and with no interruption from the commonly studied interferents in tap water and lake water samples. Notably, this simple yet visual striking strategy eliminates the need for expensive materials, intricate probe preparation, prolonged measurement time, and convoluted instrumentation. Hence, we hope this progressive research will pave the way for future advancements in the field of environmental monitoring, offering hope for enhanced safeguarding measures against harmful substances like carbaryl.

Declaration of competing interest

The authors declare that they have no known competing financial interests or personal relationships that could have influenced the work reported in this study.

CRediT authorship contribution statement

Meiling Xu: Writing – original draft. **Xinyang Li:** Writing – review & editing. **Pengyuan Liu:** Investigation. **Junjun Liu:** Data curation. **Xiao Han:** Writing – review & editing. **Guodong Chai:** Data curation. **Shuangling Zhong:** Data curation. **Bai Yang:** Writing – review & editing. **Liying Cui:** Writing – review & editing.

Acknowledgment

This work is supported by the Natural Science Foundation of the Science and Technology Department of Jilin Province (No. 20220101086JC).

Supplementary materials

Supplementary material associated with this article can be found, in the online version, at doi:10.1016/j.cclet.2024.109860.

References

[1] D.W. Miwa, G.R.P. Malpass, S.A.S. Machado, A.J. Motheo, Water Res. 40 (2006) 3281–3289.
[2] S. Ruengprapavut, T. Sophonnithiprasert, N. Pongpoungphet, Food Chem. 309 (2020) 125659.
[3] K. Zhang, J.W. Wong, P. Yang, et al., Anal. Chem. 84 (2012) 5677–5684.
[4] E. Sobhanzadeh, N.K. Abu Bakar, M.R. Bin Abas, K. Nemati, J. Hazard. Mater. 186 (2011) 1308–1313.
[5] E.Y. Yang, H.S. Shin, J. Chromatogr. A 1305 (2013) 328–332.
[6] W. Jiao, G.Y. Ding, L. Wang, Y. Liu, T.R. Zhan, Microchim. Acta 189 (2022) 78.
[7] F.E. Salih, B. Achiou, M. Ouammou, et al., J. Adv. Res. 8 (2017) 669–676.
[8] F.K. Alsammarraie, M.S. Lin, J. Agric. Food Chem. 65 (2017) 666–674.
[9] Y.X. Fan, K.Q. Lai, B.A. Rasco, Y.Q. Huang, LWT-Food Sci. Technol. 60 (2015) 352–357.
[10] H.B. Wu, L. Yang, W. Sun, P. Yang, H.L. Xing, RSC Adv. 12 (2022) 33696–33705.
[11] Q.J. Luo, Y.X. Li, M.Q. Zhang, P. Qiu, P.H. Deng, Chin. Chem. Lett. 28 (2017) 345–349.
[12] C. Zhang, H.Y. Cui, J.R. Cai, Y.Q. Duan, Y. Liu, J. Agric. Food Chem. 63 (2015) 4966–4972.
[13] H.Y. Chen, O. Hu, Y. Fan, et al., Food Chem. 327 (2020) 127075.
[14] F. Shahdost-fard, N. Fahimi-Kashani, M.R. Hormozi-nezhad, Talanta 221 (2021) 121467.
[15] Z. Zhang, Q.R. Zhang, L.F. Li, D. Lin, C.L. Jiang, ACS Sustainable Chem. Eng. 11 (2023) 4998–5006.
[16] Y.H. Yi, G.B. Zhu, C. Liu, et al., Anal. Chem. 85 (2013) 11464–11470.
[17] D.B. Liu, W.W. Chen, J.H. Wei, et al., Anal. Chem. 84 (2012) 4185–4191.
[18] J. Chen, Z.Q. Liu, J.X. Fang, et al., LWT-Food Sci. Technol. 157 (2022) 113099.
[19] H.T. Li, C.H. Sun, R. Vijayaraghavan, et al., Carbon 104 (2016) 33–39.
[20] D. Zhao, C.X. Chen, J. Sun, X.R. Yang, Analyst 141 (2016) 3280–3288.
[21] Y.Y. Chen, X. Qin, C.L. Yuan, R. Shi, Y.L. Wang, Dyes Pigm. 181 (2020) 108529.
[22] J. Wang, X.B. Sun, W. Pan, J.P. Wang, Microchem. J. 178 (2022) 107408.
[23] Y.Y. Yang, C.Y. Tong, R.R. Zhou, et al., Food Chem 431 (2024) 137127.
[24] Y.L. Liu, P.H. Zhou, Y.L. Wu, et al., Sci. Total Environ. 827 (2022) 154357.
[25] Y. Liu, J.F. Wei, X. Yan, et al., Chin. Chem. Lett. 32 (2021) 861–865.
[26] M.Y. Fang, B.Y. Wang, X.L. Qu, et al., Chin. Chem. Lett. 35 (2024) 108423.
[27] X.X. Hu, H.J. Wu, Q. Zhang, F. Gao, Chin. Chem. Lett. 34 (2023) 107846.
[28] F.L. Yuan, Y.K. Wang, G. Sharma, et al., Nat. Photonics 14 (2020) 171–176.
[29] L. Ai, Z.Q. Song, M.J. Nie, et al., Angew. Chem. Int. Ed. 62 (2023) e202217822.
[30] B.Y. Wang, H.W. Wang, Y.S. Hu, et al., Nano Lett. 23 (2023) 8794–8800.
[31] X.H. Zhao, Q.L. Tang, S.J. Zhu, et al., Nanoscale 11 (2019) 9526–9532.
[32] B.X. Cheng, Z.L. Yang, F.R. Chen, et al., Sci. Total Environ. 901 (2023) 165973.
[33] V.C. Hoang, K. Dave, V.G. Gomes, Nano Energy 66 (2019) 104093.
[34] L.L. Qin, Y.J. Guo, L.F. Li, et al., ACS Sustainable Chem. Eng. 11 (2023) 11032–11040.
[35] Q.R. Zhang, Z. Zhang, S.H. Xu, et al., J. Hazard. Mater. 436 (2022) 129320.
[36] J.H. Zhang, J. Wang, F.J. Ouyang, et al., Anal. Chim. Acta 1279 (2023) 341837.
[37] Q. Yang, J.H. Li, X.Y. Wang, H. Xiong, L.X. Chen, Anal. Chem. 91 (2019) 6561–6568.
[38] Y.J. Zhan, Y.B. Zeng, L. Li, et al., ACS Sens. 4 (2019) 1252–1260.
[39] D.D. Su, X. Zhao, X. Yan, et al., Biosens. Bioelectron. 194 (2021) 113598.
[40] Z.H. Jin, M. Liu, X.D. Huang, et al., Anal. Chem. 94 (2022) 7609–7618.
[41] Y.Q. Zhang, J.P. Wang, L. Wang, et al., Adv. Mater. 35 (2023) 2302536.
[42] Z. Han, D.Y. Nan, H. Yang, et al., Sens. Actuators B: Chem. 298 (2019) 126842.
[43] H.F. Wu, Y.B. Chen, M.Q. Xu, et al., Sci. Total Environ. 860 (2023) 160533.
[44] J.J. Liu, Y.J. Geng, D.W. Li, et al., Adv. Mater. 32 (2020) 1906641.
[45] Y.T. Wang, X.Y. Chang, N. Jing, Y. Zhang, Anal. Methods 10 (2018) 2775–2784.
[46] R.Y. Dai, X.P. Chen, Y.P. Hu, Sens. Actuators B: Chem. 382 (2023) 133499.
[47] R. Fu, H.Q. Song, X.J. Liu, et al., Chin. J. Chem. 41 (2023) 1007–1014.
[48] F.S. Shan, L.J. Fu, X.Y. Chen, et al., Chin. Chem. Lett. 33 (2022) 2942–2948.
[49] Y.F. Gao, Y. Jiao, H.L. Zhang, et al., J. Mater. Chem. B 7 (2019) 5502–5509.
[50] F. Qu, J.L. Bai, Y.Q. Zhu, et al., Phys. Chem. Chem. Phys. 25 (2023) 2762.
[51] S.Y. Tang, D. Chen, G.Q. Guo, et al., Sci. Total Environ. 825 (2022) 153913.
[52] D. Hawker, J. Chem. Educ. 92 (2015) 1531–1535.
[53] J. Ben Attig, L. Latrous, M. Zougagh, Á. Ríos, Talanta 226 (2021) 122106.
[54] M.Y. Deng, S. Wang, C.S. Liang, H.X. Shang, S.M. Jiang, RSC Adv. 6 (2016) 26936–26940.